

<https://doi.org/10.1038/s42005-024-01893-2>

Temporal-spatial manipulation of bi-focal bi-chromatic fields for terahertz radiations

Check for updates

Jingjing Zhao^{1,2}, Yizhu Zhang³✉, Yanjun Gao¹, Meng Li⁴, Xiaokun Liu⁴, Weimin Liu⁴, Tian-Min Yan¹ & Yuhai Jiang^{1,4,5}✉

Mixing the fundamental (ω) and the second harmonic (2ω) waves in the gas phase is a widely employed technique for emitting terahertz (THz) pulses. The THz generation driven by bi-chromatic fields can be described by the photocurrent model, where the THz generation is attributed to free electrons ionized by the ω field, and the 2ω field provides a perturbation to break the symmetry of the asymptotic momentum of free electrons. However, we find that the THz radiation is amplified by one order of magnitude when driven by bi-focal bi-chromatic fields, which cannot be explained only using the photocurrent model. Meanwhile, present measurements demonstrate that the THz radiation mainly originates from the plasma created by the 2ω pulses instead of the ω pulses. Energy transfer from the 2ω beam to the THz beam during the THz generation has been observed, validating the major contribution of the 2ω beam. Furthermore, the THz bandwidth has been observed to extensively exceed the bandwidth of the pump pulse, not be explained by the photocurrent model as well. These counterintuitive results present a significant challenge for understanding strong-field nonlinear optics and simultaneously expanding various applications.

The demand for super-continuum terahertz (THz) pulses, capable of encompassing a broader spectrum of fingerprint spectral lines associated with rotational and vibrational resonance transitions, is significant in both commercial and scientific applications of spectroscopic techniques. In comparison to nonlinear optical crystals emitting narrow-band THz pulses^{1–3}, mixing bi-chromatic strong laser fields in a gas-phase medium has emerged as a popular alternative for generating high-intensity super-continuum THz pulses^{4–7}. The efficiency of optics-to-THz conversion generated from ambient air plasma induced by bi-chromatic fields of 800 nm and 400 nm with a 35 fs pulse duration is approximately 0.01%⁸, and the THz bandwidth can be extended up to 40 THz⁹. To enhance the THz conversion efficiency, a longer pump wavelength can be employed^{10–14}, while a broader THz bandwidth can be generated by a few-cycle pump pulse with broader bandwidth^{15,16}.

The THz generation from bi-chromatic fields can be explained by the photocurrent model. According to this model, the THz pulse generation inside a plasma primarily results from the transient photocurrent of free electrons induced by the femtosecond field^{17–20}. Several commonly accepted perspectives can be derived from the photocurrent model: (1) free electrons are predominantly generated through ionization by the high-strength ω

pulse. The presence of the 2ω pulse as a perturbative field creates a symmetry-broken laser field, thereby introducing an asymptotic momentum of the free electrons. This asymptotic photocurrent ultimately leads to THz radiation^{21–23}. (2) The bandwidth of the THz radiation is directly proportional to the bandwidth of the pump pulse and inversely proportional to the duration of the pump pulse²⁴.

In our previous study, we reported a bi-focal geometry involving two cascading plasmas, which revealed enhanced THz radiation with a bandwidth of up to 100 THz and a conversion efficiency of $\sim 0.1\%$ ²⁵. This phenomenon challenges the common-sense cognition that generating high-intensity super-continuum THz radiation requires pump pulses of longer wavelengths and wider bandwidths, as suggested by the photocurrent model. In this article, our aim is to exert experimental control over THz generation through the temporal-spatial manipulation of bi-focal bi-chromatic fields, thereby attempting to explain this counter-intuitive experimental phenomenon. Compared to our previous paper, this paper introduces temporal manipulation of the bi-chromatic pulses. It demonstrates that THz strength can be enhanced by 13 times when the two cascading foci are displaced compared to when they are overlapped. Meanwhile, we analyze firstly the relationship between the THz and 2ω

¹Shanghai Advanced Research Institute, Chinese Academy of Sciences, Shanghai, China. ²University of Chinese Academy of Sciences, Beijing, China. ³School of Electrical Engineering, Tiangong University, Tianjin, China. ⁴Center for Transformative Science and School of Physical Science and Technology, ShanghaiTech University, Shanghai, China. ⁵School of Physics, Henan Normal University, Xinxiang, China. ✉e-mail: zhangyizhu@tju.edu.cn; jiangyh3@shanghaitech.edu.cn

spectra, observing the energy transfer between them. Furthermore, we measure the spatial location of the THz emission along the plasma filaments and discover that the THz radiation primarily emits from the 2ω plasma filament. As well, the dependence of the THz intensity on the laser intensity is investigated. These counterintuitive experimental results cannot be explained solely by relying on the photocurrent model. The present experimental findings, explored across multiple dimensions, pose significant challenges for theoretical investigations.

Methods

In the experiment, we conducted joint measurements between THz generation and third-order harmonic (TH) generation when linearly polarized bi-chromatic fields are parallelly aligned. The experimental setup is depicted in Fig. 1. A Ti:sapphire femtosecond amplification laser system delivers 40 fs (full width at half maximum (FWHM)) light pulses centered at $\omega = 810$ nm with a maximal pulse energy of 1.7 mJ. The 2ω pulse is produced by the ω pulse after passing through a β -barium borate (BBO) crystal with a thickness of 200 μm and type-I phase-matching condition. This process yields an up-conversion efficiency of $\sim 30\%$. Subsequently, the $\omega - 2\omega$ fields are split by a dichroic mirror (DM2) into two arms of a Mach-Zehnder interferometer. In this setup, the time delay, relative orientation of polarization, and focus conditions of $\omega - 2\omega$ fields can be controlled, respectively. To suppress phase jitter between the $\omega - 2\omega$ beams, an actively stabilized Mach-Zehnder interferometer is employed. This stabilization is achieved by introducing a continuous green laser (532 nm) that co-propagates with the $\omega - 2\omega$ beams and generates interference. The interference fringes are monitored by a CCD camera, serving as a feedback signal. Real-time stabilization is facilitated by a mirror mounted on a piezo actuator that provides continuous feedback to maintain stable interference fringes. Upon stabilization, the relative phase fluctuation in the system remains below 0.02π . After passing through the actively stabilized Mach-Zehnder interferometer, the $\omega - 2\omega$ beams are combined by another dichroic mirror (DM3) to induce gas plasma ionization.

The spatial manipulation of $\omega - 2\omega$ pulses can be achieved by placing two lenses with a focal length of 100 mm (lens1, lens2) in each arm of the Mach-Zehnder interferometer. The lens for the 2ω pulse is mounted on a translation stage (Stage2), facilitating the fine-tuning of the spatial separation (d) between the foci of $\omega - 2\omega$ beams. The temporal separation (τ) of bi-chromatic pulses can be practically controlled through two methods, including fine-tuning with sub-femtosecond accuracy and coarse-tuning

with femtosecond accuracy. In the fine-tuning method, τ can be adjusted by introducing different co-propagating optical pathways for $\omega - 2\omega$ beams due to the difference in refractive indices between the two pulses in the air. In addition, τ can also be coarsely changed by moving the piezo actuator in one arm of the interferometer.

The non-collinear propagation, resulting from the beam splitting and recombination of the bi-chromatic beams, disrupts the conical spatial distribution of the THz beam profile emitted along the forward direction. To address this misalignment issue, the THz beam profile is detected using a THz camera. In Supplementary Note 1, the THz beam profiles are presented to showcase the successful collimation of the bi-chromatic beams at $d = 0$ mm, $d = 1$ mm, and $d = 2$ mm, respectively.

In the detection setup, the ω pulse and 2ω pulse after focusing as well as the generated TH, are reflected by a polished silicon wafer and dispersed by a prism. The ω and 2ω beams are blocked by an iris serving as a spatial filter, allowing only the TH to couple into the fiber optic spectrometer (Thorlabs CCS200). The ω and 2ω spectra are measured in the same manner. Subsequently, the transmitted THz is collimated and focused by two off-axis parabolic mirrors (OPM1, OPM2, 100 mm focal length) and detected by a pyroelectric detector (PED, THZ9B-BL Gentec-EO). In the experimental setup, two 45-degree undoped silicon wafers are used. One silicon wafer is located between DM3 and OPM1 to filter out the residual laser, with a THz transmission efficiency of $\sim 70\%$. The other silicon wafer is located between OPM1 and M3 to reflect the THz radiation, with a THz reflection efficiency of $\sim 30\%$. These two silicon wafers result in an overall THz propagation efficiency of $\sim 20\%$. During the measurement, the intensities of THz and TH can be jointly recorded as a function of d and τ of $\omega - 2\omega$ pulses.

The THz spectra are measured using a Fourier transform spectrometer based on the principle of a Michelson interferometer equipped with a $2\ \mu\text{m}$ thick pellicle beam splitter (BS) and two THz mirrors (M1, M2). The THz waves passing through the Michelson interferometer are focused by an off-axis parabolic mirror (OPM3, 100 mm focal length) and detected by a pyroelectric detector. The Fourier transform spectrometer exhibits a flat response function above 15 THz. The THz spectra below 15 THz are not sufficiently accurate, which is attributed to the non-flat frequency response of PEDs. We obtain the low-frequency THz spectra vs d through electro-optical sampling, as demonstrated in Supplementary Note 6. Wavelength calibration is conducted using an optical parametric amplifier with precisely defined wavelengths. Further details of the calibration process are presented in Supplementary Note 2.

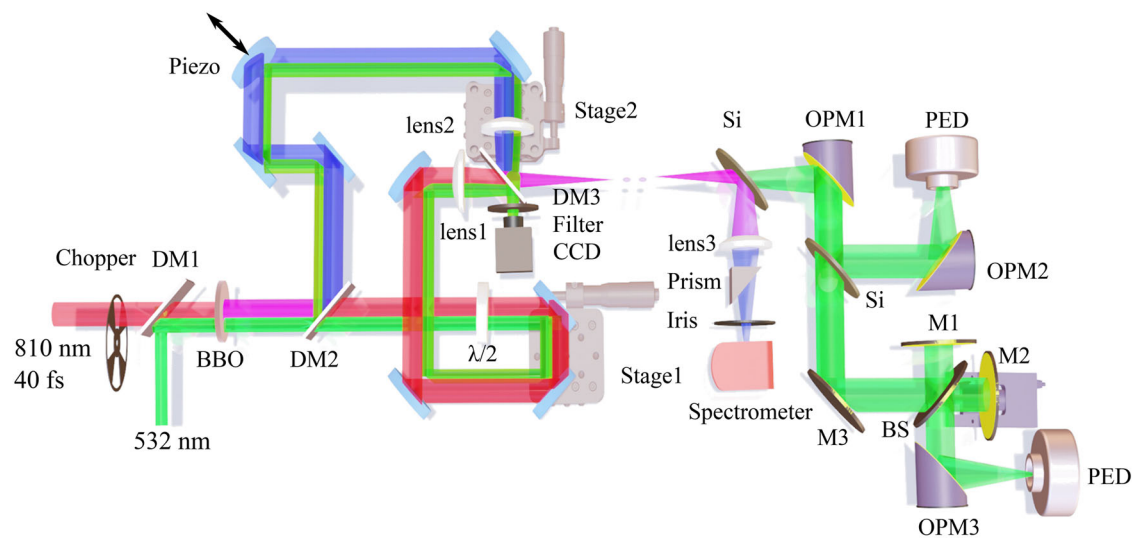


Fig. 1 | Schematic diagram of THz amplification. The TH radiation is recorded by a spectrometer. The intensity and spectra of THz can be detected using the pyroelectric detector and a home-built Fourier transform spectrometer system. DM1–3 dichroic mirror, BBO type-I β -barium borate crystal, Stage1–2 translation stage, $\lambda/2$

half-wave plate, CCD CMOS camera detector, Piezo piezo stage, Si silicon wafer, OPM1–3 off-axis parabolic mirror, BS pellicle beam splitter, M1–3 THz mirror, PED pyroelectric detector.

Results and discussion

THz waves and TH amplification via temporal-spatial manipulation

Figure 2a depicts the TH intensity $I_{TH}(d, \tau)$ vs temporal-spatial manipulation and the calibration of the zero delays of $\omega - 2\omega$ pulses. Experimentally, we also determine zero time delay by some experimental phenomena: (i) the fluorescence strength of the 2ω plasma filament suddenly decreases at $\tau = 0$ fs. (ii) Significant interference fringe is observed in the super-continuum spectra generated by the ω and 2ω plasmas at $\tau = 0$ fs. When referring to $\tau > 0$ fs, it indicates that the 2ω pulse temporally precedes the ω pulse. For $d > 0$ mm, it means that the plasma induced by the 2ω pulse is spatially located past the plasma induced by the ω pulse along the laser propagation direction. The τ corresponding to the maximum TH yield is defined as the zero delay. $I_{THz}(\tau)$ and $I_{TH}(\tau)$ with sub-femtosecond time delay, as well as the determination of the zero delays for the bi-chromatic fields specifically are provided in Supplementary Note 3. $I_{THz}(\tau)$ and $I_{TH}(\tau)$ exhibit anti-correlated behavior as a function of sub-femtosecond time delay, consistent with the previous measurements^{20,26}.

In Fig. 2b, the distribution of THz intensity $I_{THz}(d, \tau)$ presents a lobe landscape in the dimensions of spatial d and temporal τ separations. Experimental THz intensity $I_{THz}(d, \tau)$ very sensitively depends on changes of d and τ , where a maximum distribution illuminates at certain d and τ values. It reveals two counter-intuitive features that warrant attention: (i) in the temporal dimension as shown in Fig. 2c, the maximum THz generation appears when the bi-chromatic pulses are temporally separated. By scanning the time delay with femtosecond accuracy, we note that I_{THz} is insensitive vs τ at $d = 0$ mm, where a broad distribution at about $\tau \approx -25$ fs and 100 fs is observed. However, peaked maxima of $I_{THz}(\tau)$ at increasing time delays τ is more and more pronounced as d increases and optimally I_{THz} with a 13 times high is achieved in Fig. 2c at $d = 2.5$ mm and $\tau = 58$ fs in comparison to that at $d = 0$ mm and $\tau = 0$ fs. The THz power generated by the bi-chromatic fields reaches ~ 1.4 mW. (ii) In the spatial dimension as shown in Fig. 2d, efficient optimization of THz generation occurs when the foci of bi-chromatic beams are noticeably separated. The maximum I_{THz} does not occur at $d = 0$ mm, and I_{THz} is more efficient when $d > 0$ mm compared to $d < 0$ mm. The analogy to the THz intensity dependence of two-pulse time delays shown in Fig. 2c, peaked maximum distributions $I_{THz}(d)$ shift to larger spatial separation d as τ increases.

These findings contrast with conventional expectations, where one would anticipate the THz yield to be optimized when the foci of the $\omega - 2\omega$ beams are spatially and temporally overlapped. These observations are counter to the common expectation that the temporal and spatial overlapping of the bi-chromatic pulses would be a prerequisite for the most efficient THz generation and the ω laser is mainly responsible for the THz generation.

According to the conventional understanding, both TH and THz radiation can be attributed to the Brunel radiation mechanism within the framework of the single-electron approximation^{17,18,27,28}. For the case of present two-foci cascading plasma in time and in space, the most likely scenarios are as follows: The 2ω plasma filament plays a dominating role in THz generation (see the ‘‘Spectral measurements of Bi-chromatic pulses’’ subsection in the ‘‘Results and discussion’’), where two color lasers are still prerequisites for highly efficient THz generation and the ω laser provides field modulation resulting in the symmetry breaking of a combined $2\omega - \omega$ field. To a large extent presents a two-foci cascading plasma configuration, where 2ω travels ahead in time and is focused ahead in space considering laser propagation direction, enabling to avoid THz absorption by the ω created plasma. Furthermore, in qualitative analysis, the broadening of the 2ω spectra is likely due to nonlinear effects and dispersion during laser propagation, resulting in pulse self-compression. Simultaneously, the plasma dispersion may also cause an additional delay in the pulses, which can be compensated by the delay introduced in the Mach-Zehnder interferometer.

Theoretical calculations²⁵ on the spatial modulation of bifocal field attributed to plasma absorption. In the present spatial geometry of two-foci, the ω laser field at the focus spot of 2ω laser is relatively stronger only if $\tau > 0$ fs in comparison to $\tau \leq 0$ fs. That is to say that the optimal magnitudes of temporal and spatial separations for the highest THz emission will also be affected by laser profiles like intensity and pulse duration etc.

Spectral measurements of Bi-chromatic pulses

To gain insight into the origin of the enhancement of THz waves in the temporal-spatial manipulation of bi-chromatic fields, we measured the spectra of the bi-chromatic fields after focusing and the THz spectra emitted by the bi-chromatic fields at different d , which are shown in Fig. 3. The ω spectra vs d are presented in Fig. 3a, and we do not observe any shift in the ω spectra after focusing. Furthermore, Fig. 3a suggests that the full width at half maximum (FWHM) of the ω spectrum (~ 25 nm), reasonably supports a Fourier-transform-limited pulse with a pulse duration of ~ 40 fs. Conversely, the red arrow in Fig. 3b indicates that the intensity of the 2ω spectra increases with d , along with a broadening on the red side of the 2ω spectra from $d = 0$ mm to $d = 3$ mm. The 2ω spectrum at large negative d in Fig. 3b can be considered as the original 2ω spectrum. The original 2ω spectrum is presented in Supplementary Note 7. According to the original 2ω spectrum of ~ 3 nm in FWHM, the pulse duration of the 2ω pulse is estimated to be ~ 80 fs. It’s worth noting that non-zero frequency detuning may occur naturally during the propagation of strong-field pulses. For example, the frequency shift due to plasma is a blue shift, and the Kerr effect is a red shift at the leading edge of the intensity^{29,30}. The ω and 2ω spectra are depicted as a function of d , illustrating that the ω pulse serves solely as a perturbation

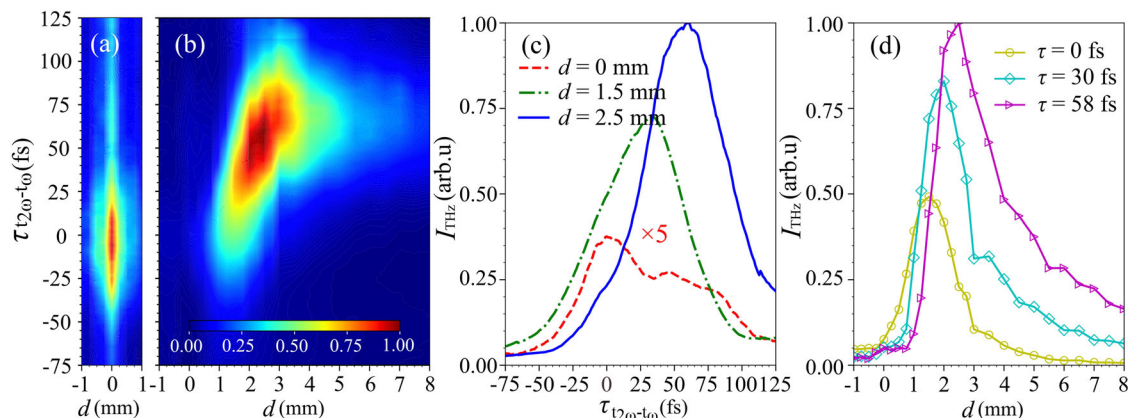


Fig. 2 | Temporal and spatial modulation of THz waves and TH generation under bi-chromatic fields. **a** Measured TH intensity $I_{TH}(d, \tau)$ vs the d and τ . **b** The distribution of THz intensity $I_{THz}(d, \tau)$ as a function of d and τ . **c** The THz intensities $I_{THz}(\tau)$ projected from **(b)** at $d = 0$ mm (red dashed line), $d = 1.5$ mm (green dash

dotted line), and $d = 2.5$ mm (blue solid line), respectively. **d** The THz intensities $I_{THz}(d)$ projected from **(b)** at $\tau = 0$ fs (yellow circles), $\tau = 30$ fs (cyan diamonds), and $\tau = 58$ fs (magenta right triangles), respectively.

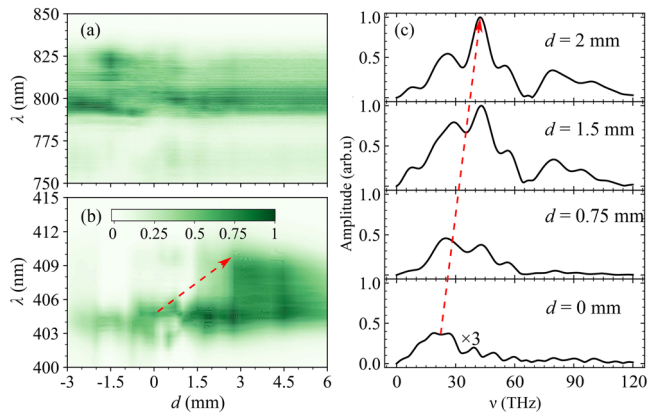


Fig. 3 | The normalized spectra of ω , 2ω , and THz pulses at $\tau = 0$ fs. **a** The normalized spectra of ω emitted from plasma filament vs d . **b** The normalized spectra of 2ω emitted from plasma filament vs d , where the red arrow indicates the redshift of 2ω spectra. The color bar in panel (b) refers also to panel (a). **c** The THz spectra for $d = 0$ mm, $d = 0.75$ mm, $d = 1.5$ mm, and $d = 2$ mm, respectively, where the red arrow indicates the blue shift of THz spectra.

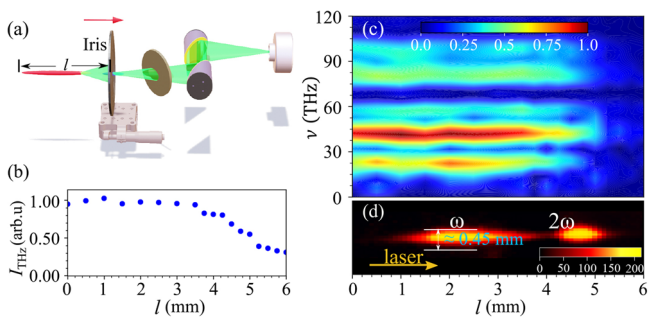


Fig. 4 | The spatial location of THz emission on the plasma filament. **a** Measurement schematic of the spatial location of THz emission along the plasma filament. An iris with an aperture diameter of 0.5 mm is moved along the laser propagation axis, aligning with the plasma filament (depicted in red) passing through the aperture. As the iris is positioned, it effectively blocks the THz beam (depicted in green) emitted from the plasma filament on the left side of the iris. **b** THz intensity $I_{\text{THz}}(l)$, measured with the PED as a function of the iris position l is shown as blue circles. **c** As the iris moves, THz spectra are measured for emissions originating from the plasma filament on the right side of the iris. **d** Snapshot of the fluorescence obtained by the CCD camera at $d = 2$ mm and $\tau = 0$ fs. The diameter of the plasma filament is ~ 0.45 mm. We label the positions of the plasma filaments generated by ω and 2ω pulses using ω and 2ω .

during the THz generation process. It is observed that laser nonlinear propagation has a greater impact on the 2ω pulse compared to the ω pulse.

Furthermore, from the results of THz spectra vs d in Fig. 3c, it can be observed that the peak of THz spectra shifts from 20 THz to 45 THz as d increases from 0 mm to 2 mm, as depicted by the red arrow. This blue shift is accompanied by a broadening of the THz spectra bandwidth by a factor of 6 compared to the ω spectra bandwidth. The red shift of the 2ω spectra and the blue shift of the THz spectra demonstrate the energy transfer from the 2ω beam to the THz beam in the THz generation process. Whether based on the four-wave-mixing (FWM) process ($\omega + \omega - 2\omega$) or the photocurrent model, it is indicated that the broadening of 2ω spectra on the red side, driven by bi-chromatic laser fields, leads to a shift of the radiated THz pulses towards the high-frequency side^{31,32}. Our experimental results are consistent with the theoretical description.

Spatial location of THz radiation

We conducted investigations on THz emission from various segments of the plasma filament, enabling us to pinpoint the spatial location of THz

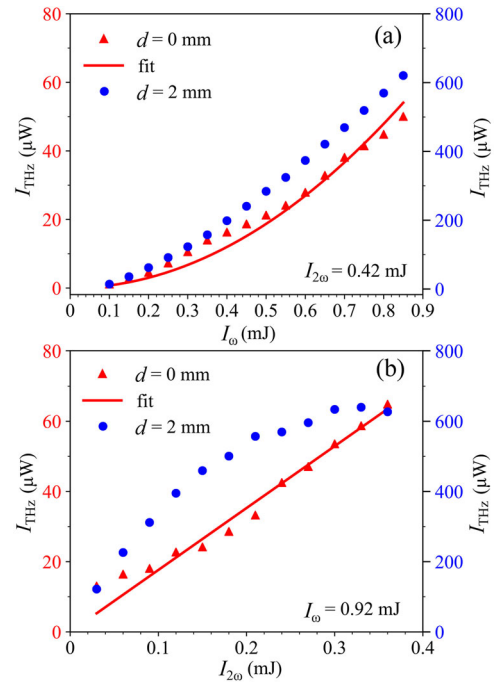


Fig. 5 | Intensity-dependent calibration of THz yield. **a** THz intensity I_{THz} (THz power accounting for attenuation by two Si wafers), measured with PED, is presented as a function of the ω pulse energy I_ω , while keeping the 2ω pulse energy $I_{2\omega}$ constant at 0.42 mJ. **b** The I_{THz} is depicted as a function of $I_{2\omega}$, with the I_ω set at 0.92 mJ. The red triangles represent I_{THz} vs I_ω and $I_{2\omega}$ at $d = 0$ mm and the blue circles represent I_{THz} vs I_ω and $I_{2\omega}$ at $d = 2$ mm, they correspond to the red and blue scales, respectively. The red solid line represents the fitting result of I_{THz} vs I_ω and $I_{2\omega}$ at $d = 0$ mm.

emission along the plasma filament, and gain valuable insights into the underlying mechanism driving THz amplification. The experimental schematic is shown in Fig. 4a. An iris with an aperture diameter of 0.5 mm, concentric with the plasma filament, is moved along the propagation axis of the bi-chromatic beams. The efficacy of a 0.5 mm aperture iris in isolating THz emissions is calculated in Supplementary Note 1, which indicates that the THz radiation emitted by plasma segments that are more than 0.75 mm away from the aperture can be totally blocked. The THz radiation emitted by plasma segments that are less than 0.75 mm away from the aperture partially passes through the aperture. Moreover, the aperture diameter is set at 0.5 mm, which is attributed to the plasma diameter of ~ 0.45 mm, as illustrated in Fig. 4d. A 0.5 mm aperture is chosen to ensure that the propagation of the plasma filament is not disturbed. A smaller aperture will cut the plasma filament. In Fig. 4, the plasma filament generated by the bi-chromatic fields is fixed in both spatial and temporal dimensions at $d = 2$ mm and $\tau = 0$ fs. The plasma fluorescence image is presented in Fig. 4d.

The THz intensity $I_{\text{THz}}(l)$ as a function of iris position l is illustrated in Fig. 4b, where $l = 0$ mm is defined as the starting position of measurement. When the iris is positioned at the location of the plasma filament generated by the ω pulse, the detected THz intensity remains constant vs l . However, a sudden decrease in THz intensity is observed when blocking the THz emission from the 2ω plasma filament, implying that the majority of THz pulses are generated from the 2ω plasma filament rather than the ω plasma filament. Generally, the photocurrent model indicates that the ω plasma filament is more likely to emit THz due to its higher intensity compared to the 2ω pulse. However, the surprising experimental finding indicates that THz generation is actually from the 2ω plasma filament with lower electron density. This difference between theory and experimental observations highlights the necessity for a deeper investigation into the mechanisms underlying THz generation in ω and 2ω plasma filaments. Here, we consider

that the ω pulse plays an assisting role in the THz radiation process, and the propagation of the 2ω pulse is altered at the 2ω focus due to certain nonlinear effects, which in turn radiates THz pulses at the 2ω plasma position^{33,34}. Meanwhile, the THz spectra as a function of l are measured using a Fourier transform spectrometer while translating the iris position l , and the results are illustrated in Fig. 4c. Employing the differential approach, the spectral distribution radiated from different segments of the plasma filament is presented in Supplementary Note 4. The high-frequency components of THz waves predominantly originate from the 2ω plasma filament, particularly the end of the 2ω plasma filament.

Intensity-dependent calibration

Since our experimental arrangement permits us to adjust the energy of ω and 2ω beams individually, direct measurements of the emitted THz intensity I_{THz} vs I_ω at $d = 0$ mm and $d = 2$ mm, respectively, as depicted in Fig. 5a. We also demonstrate the dependency of I_{THz} on $I_{2\omega}$ at $d = 0$ mm and $d = 2$ mm, respectively, as shown in Fig. 5b. During the measurement, the energy of one beam is fixed while the energy of the other beam is changed. Typically, in the case of bifocal overlap ($d = 0$ mm) was reported previously^{35–37}: $E_{\text{THz}} \propto E_{2\omega} E_\omega^2$. Since the THz intensity is proportional to the square of the THz electric field, i.e. $I_{\text{THz}} \propto E_{\text{THz}}^2$, $E_{\text{THz}} \propto E_{2\omega} E_\omega^2$ can be rewritten as:

$$I_{\text{THz}} \propto I_{2\omega} I_\omega^2. \quad (1)$$

The red solid line in Fig. 5a, b represents the fitted results of I_{THz} vs I_ω and $I_{2\omega}$, respectively. These results are obtained from Eq. (1) combined with experimental data. This analysis corresponds to the case where $d = 0$ mm. As predicted by the theory, the emitted I_{THz} is proportional to the square of I_ω (as observed in Fig. 5a) and to $I_{2\omega}$ above the ionization threshold (as observed in Fig. 5b). The observed dependence of I_{THz} on I_ω and $I_{2\omega}$ at $d = 0$ mm is consistent with the conventional results.

Simultaneously, we measured the I_{THz} vs I_ω and $I_{2\omega}$ at $d = 2$ mm, respectively. The results demonstrate that I_{THz} is proportional to the square of the I_ω at $d = 2$ mm, which is consistent with the trend observed at $d = 0$ mm. However, the relationship between I_{THz} and $I_{2\omega}$ shows a rapid increase followed by a slow increase, deviating from the trend at $d = 0$ mm. To confirm that this phenomenon is not exclusive to high laser intensities, we decreased the ω and 2ω laser intensity to explore the relationship between THz intensity and laser intensity. The observation reveals that the phenomenon persists under lower laser intensity (for more details, see Supplementary Note 5). Thus, another solid piece of evidence is provided here that the increase in THz intensity at $d = 2$ mm is due to the influence of the 2ω pulse.

Based on the aforementioned observations, it can be concluded that 2ω pulse plays a crucial role in both the enhancement and broadening of THz waves. An attempt was made to simulate the experiment using 3D propagation equations^{38,39}; however, a comprehensive elucidation of the experimental results cannot be achieved at present. We hypothesize that the four-wave mixing of ω and 2ω frequency components in both air and plasma is not accurately reproduced in the simulation. The presence of numerous nonlinear channels generating new frequency components, corresponding to nonlinear coefficients such as $\chi(2\omega: 2\omega, -\omega, \omega)$, $\chi(2\omega: 2\omega, -2\omega, 2\omega)$, etc., in the air and plasma mixture complicates the precise determination of these nonlinear coefficients. As a result, a more thorough theoretical explanation is needed.

Conclusion

In conclusion, our measurements reveal that THz generation is significantly optimized through the temporal-spatial manipulation of bi-chromatic fields. This optimization occurs when the two cascading foci are displaced, and temporal separation of the bi-chromatic pulses is introduced. By employing temporal and spatial modulation of the bi-focal bi-chromatic fields, the I_{THz} is amplified by a factor of 13 compared to the conventional bi-chromatic THz generation, while the bandwidth of THz extends 6 times

beyond the pump light bandwidth. Meanwhile, detailed experiments have revealed counterintuitive phenomena: (1) photon energy transfer from the 2ω beam to the THz beam is elucidated through 2ω and THz spectral correlation measurements; (2) the measurements of the location of THz emission from the plasma filament have revealed that the THz pulse originates from the 2ω plasma filament rather than the higher-electron-density ω plasma filament; and (3) the investigation of the THz intensity dependence on the laser intensity reveals that when the two foci are pulled apart ($d = 2$ mm), the dependence between I_{THz} and $I_{2\omega}$ clearly goes beyond the conventional scaling relationship. These multi-perspective observations, which cannot be solely explained by the conventional photocurrent model, call for further theoretical investigations to offer comprehensive explanations and demonstrate potential applications in spectroscopic research.

Data availability

Data underlying the results presented in this paper are not publicly available at this time but can be obtained from the authors upon reasonable request.

Received: 1 March 2024; Accepted: 2 December 2024;

Published online: 19 December 2024

References

- Zhang, X.-C. et al. Terahertz optical rectification from a nonlinear organic crystal. *Appl. Phys. Lett.* **61**, 3080–3082 (1992).
- Han, P. Y., Tani, M., Pan, F. & Zhang, X.-C. Use of the organic crystal DAST for terahertz beam applications. *Opt. Lett.* **25**, 675–677 (2000).
- Vicario, C. et al. Generation of 0.9-mJ THz pulses in DSTMS pumped by a Cr:Mg₂SiO₄ laser. *Opt. Lett.* **39**, 6632–6635 (2014).
- Cook, D. J. & Hochstrasser, R. M. Intense terahertz pulses by four-wave rectification in air. *Opt. Lett.* **25**, 1210–1212 (2000).
- Fülöp, J. A., Tzortzakakis, S. & Kampfrath, T. Laser-driven strong-field terahertz sources. *Adv. Opt. Mater.* **8**, 1900681 (2020).
- Liao, G. & Li, Y. Perspectives on ultraintense laser-driven terahertz radiation from plasmas. *Phys. Plasmas* **30**, 090602 (2023).
- Simpson, T. T. et al. Spatiotemporal control of two-color terahertz generation. *Phys. Rev. Res.* **6**, 013041 (2024).
- Oh, T. I. et al. Intense terahertz generation in two-color laser filamentation: energy scaling with terawatt laser systems. *N. J. Phys.* **15**, 075002 (2013).
- Hah, J. et al. Enhancement of THz generation by feedback-optimized wavefront manipulation. *Opt. Express* **25**, 17271–17279 (2017).
- Wang, W.-M. et al. Efficient terahertz emission by mid-infrared laser pulses from gas targets. *Opt. Lett.* **36**, 2608–2610 (2011).
- Jang, D. et al. Efficient terahertz and Brunel harmonic generation from air plasma via mid-infrared coherent control. *Optica* **6**, 1338–1341 (2019).
- Koulouklidis, A. D. et al. Observation of extremely efficient terahertz generation from mid-infrared two-color laser filaments. *Nat. Commun.* **11**, 292 (2020).
- Mitrofanov, A. V. et al. Ultraviolet-to-millimeter-band supercontinua driven by ultrashort mid-infrared laser pulses. *Optica* **7**, 15–19 (2020).
- Nikolaeva, I. A. et al. Scaling law of THz yield from two-color femtosecond filament for fixed pump power. *Photonics* **9**, 974 (2022).
- Thomson, M. D., Blank, V. & Roskos, H. G. Terahertz white-light pulses from an air plasma photo-induced by incommensurate two-color optical fields. *Opt. Express* **18**, 23173–23180 (2010).
- Matsubara, E., Nagai, M. & Ashida, M. Ultrabroadband coherent electric field from far infrared to 200 THz using air plasma induced by 10 fs pulses. *Appl. Phys. Lett.* **101**, 011105 (2012).
- Zhang, K. et al. Experimental evidence for terahertz emission of continuum electrons in the dual-color laser field. *Opt. Lett.* **45**, 1838–1841 (2020).
- Zhang, K., Zhang, Y., Wang, X., Yan, T.-M. & Jiang, Y. H. Continuum electron giving birth to terahertz emission. *Photonics Res.* **8**, 760–767 (2020).

19. Gao, Y. et al. Coulomb potential determining terahertz polarization in a two-color laser field. *Opt. Lett.* **48**, 2575–2578 (2023).
20. Fan, X., Gao, Y., Yan, T.-M., Jiang, Y. & Zhang, Y. Trajectory analysis for low-order harmonic generation in two-color strong laser fields. *Opt. Express* **31**, 86–94 (2023).
21. Kim, K.-Y., Glowina, J. H., Taylor, A. J. & Rodriguez, G. Terahertz emission from ultrafast ionizing air in symmetry-broken laser fields. *Opt. Express* **15**, 4577–84 (2007).
22. Sun, W., Wang, X. & Zhang, Y. Terahertz generation from laser-induced plasma. *Opto-Electron. Sci.* **1**, 220003 (2022).
23. Yu, Z. et al. Anti-correlated plasma and THz pulse generation during two-color laser filamentation in air. *Ultrafast Sci.* **2022**, 9853053 (2022).
24. Koulouklidis, A. D., Fedorov, V. Y. & Tzortzakis, S. Spectral bandwidth scaling laws and reconstruction of THz wave packets generated from two-color laser plasma filaments. *Phys. Rev. A* **93**, 033844 (2016).
25. Zhang, Y. et al. Intensity-surged and bandwidth-extended terahertz radiation in two-foci cascading plasmas. *Opt. Lett.* **47**, 3816–3819 (2022).
26. Meng, C. et al. Phase dependence of third-order harmonic generation in gases induced by two-color laser field. *Chin. Opt. Lett.* **21**, 050201 (2023).
27. Brunel, F. Harmonic generation due to plasma effects in a gas undergoing multiphoton ionization in the high-intensity limit. *J. Opt. Soc. Am. B* **7**, 521–526 (1990).
28. He, T. et al. Third-order harmonic generation in a bi-chromatic elliptical laser field. *Opt. Express* **29**, 21936–21946 (2021).
29. Gong, C., Kawayama, I., Murakami, H., Teramoto, T. & Tonouchi, M. Intensity-dependent self-induced dual-color laser phase modulation and its effect on terahertz generation. *Sci. Rep.* **11**, 498 (2021).
30. Huang, H.-h et al. Spatio-temporal control of THz emission. *Commun. Phys.* **5**, 134 (2022).
31. Babushkin, I. et al. Tailoring terahertz radiation by controlling tunnel photoionization events in gases. *N. J. Phys.* **13**, 123029 (2011).
32. Fan, Z., Lu, C. & Liu, Y. Tunable broadband THz emission from air plasma pumped by femtosecond pulses composed of a fundamental frequency with its detuned second harmonic. *Opt. Commun.* **505**, 127532 (2022).
33. Huang, H.-h, Nagashima, T. & Hatanaka, K. Shockwave-based THz emission in air. *Opt. Express* **31**, 5650–5661 (2023).
34. Hur, M. S. et al. Laser pulse compression by a density gradient plasma for exawatt to zettawatt lasers. *Nat. Photonics* **17**, 1074–1079 (2023).
35. Kress, M., Löffler, T., Eden, S., Thomson, M. & Roskos, H. G. Terahertz-pulse generation by photoionization of air with laser pulses composed of both fundamental and second-harmonic waves. *Opt. Lett.* **29**, 1120 (2004).
36. Xie, X., Dai, J. & Zhang, X.-C. Coherent control of THz wave generation in ambient air. *Phys. Rev. Lett.* **96**, 075005 (2006).
37. Clough, B., Dai, J. & Zhang, X.-C. Laser air photonics: beyond the terahertz gap. *Mater. Today* **15**, 50–58 (2012).
38. Bergé, L., Skupin, S., Köhler, C., Babushkin, I. & Herrmann, J. 3D numerical simulations of THz generation by two-color laser filaments. *Phys. Rev. Lett.* **110**, 073901 (2013).
39. Tailliez, C. et al. Terahertz pulse generation by two-color laser fields with circular polarization. *N. J. Phys.* **22**, 103038 (2020).

Acknowledgements

This work was supported by the National Key Research and Development Program of China (no. 2022YFA1604302) and the National Natural Science Foundation of China (nos. 12334011, 12174284, and 12374262). We extend our gratitude to Stefan Skupin from Claude Bernard University Lyon 1 for his valuable contributions and engaging discussions.

Author contributions

Experiments were designed by Jingjing Zhao, Yizhu Zhang, and Yuhai Jiang. Jingjing Zhao conducted the experiments with assistance from Yizhu Zhang, Yanjun Gao, Meng Li, and Xiaokun Liu. Weimin Liu provided mid-infrared sources to calibrate the THz Fourier transform spectrometer. Experimental data were analyzed and discussed by Jingjing Zhao, Yizhu Zhang, Tian-Min Yan, and Yuhai Jiang. The manuscript was prepared by Jingjing Zhao, Yizhu Zhang, and Yuhai Jiang after discussions and input from all authors.

Competing interests

The authors declare no competing interests.

Additional information

Supplementary information The online version contains supplementary material available at <https://doi.org/10.1038/s42005-024-01893-2>.

Correspondence and requests for materials should be addressed to Yizhu Zhang or Yuhai Jiang.

Peer review information *Communications Physics* thanks the anonymous reviewers for their contribution to the peer review of this work. A peer review file is available.

Reprints and permissions information is available at <http://www.nature.com/reprints>

Publisher's note Springer Nature remains neutral with regard to jurisdictional claims in published maps and institutional affiliations.

Open Access This article is licensed under a Creative Commons Attribution-NonCommercial-NoDerivatives 4.0 International License, which permits any non-commercial use, sharing, distribution and reproduction in any medium or format, as long as you give appropriate credit to the original author(s) and the source, provide a link to the Creative Commons licence, and indicate if you modified the licensed material. You do not have permission under this licence to share adapted material derived from this article or parts of it. The images or other third party material in this article are included in the article's Creative Commons licence, unless indicated otherwise in a credit line to the material. If material is not included in the article's Creative Commons licence and your intended use is not permitted by statutory regulation or exceeds the permitted use, you will need to obtain permission directly from the copyright holder. To view a copy of this licence, visit <http://creativecommons.org/licenses/by-nc-nd/4.0/>.

© The Author(s) 2024